communications chemistry

Article

https://doi.org/10.1038/s42004-024-01334-9

On the similar spectral manifestations of protonic and hydridic hydrogen bonds despite their different origin

Check for updates

Maximilián Lamanec [1,2], Svatopluk Civiš [3] ✉ & Pavel Hobza [1,2] ✉

Previously studied complexes with protonic and hydridic hydrogen bonds exhibit significant similarities. The present study provides a detailed investigation of the structure, stabilization, electronic properties, and spectral characteristics of protonic and hydridic hydrogen bonds using low-temperature infrared (IR) spectroscopy and computational methods. Complexes of pentafluorobenzene with ammonia ($C_6F_5H\cdots NH_3$) and triethylgermane with trifluoroiodomethane ($Et_3GeH\cdots ICF_3$) were analyzed using both experimental and computational tools. Additionally, 30 complexes with protonic hydrogen bonds and 30 complexes with hydridic hydrogen bonds were studied computationally. Our findings reveal that, despite the opposite atomic charges on the hydrogens in these hydrogen bonds, and consequently the opposite directions of electron transfer in protonic and hydridic hydrogen bonds, their spectral manifestations - specifically, the red shifts in the X–H stretching frequency and the increase in intensity - are remarkably similar. The study also discusses the limitations of the current IUPAC definition of hydrogen bonding in covering both types of H-bonds and suggests a way to overcome these limitations.

Non-covalent interactions determine not only the physicochemical properties of molecular clusters and condensed molecular matter but also the structure and properties of larger macro- and biomacromolecules[1–4]. Among the various types of non-covalent interactions, hydrogen (H)-bonding plays a key role. Understanding H-bonding is thus essential for many fields of natural science. Recognizing its importance, the IUPAC introduced a definition in 2011 that encompasses not only the standard, red-shifted H-bonding but also the blue-shifting H-bonding discovered and described at the end of the 20th century[5–7]. This definition, like any other, aims to be simple and unambiguous, and for a long time, it was believed that the IUPAC definition of H-bonding met these criteria.

Previous studies[8–14], including our recent ones[15,16] have identified some ambiguities in this definition. Specifically, according to the 2011 IUPAC definition of an X-H···Y hydrogen bond, the hydrogen atom bears a partial positive charge because it is covalently bound to a more electronegative atom[7]. Among the 92 stable elements of the periodic table, only nine (C, N, O, F, Cl, Br, I, S, Se) are more electronegative than hydrogen, while the rest are more electropositive. These hydrogens, with partial negative charges, are called hydridic. The different character of hydrogen, depending on whether it is covalently bound to a more or less electronegative atom, results in different electronic properties, including the direction of intermolecular charge transfer (CT).

In protonic X-H…Y H-bonds, atom or group of atoms Y is an electron donor, and CT is directed from Y to X-H. In hydridic H-bonds, the situation is mostly opposite: X-H is an electron donor, and Y is an electron acceptor, meaning the CT is directed from X-H to Y. Despite the different charges on hydrogen leading to opposite directions of CT, the spectral presentations of protonic and hydridic H-bonds are very similar. In both cases, the X-H bond is elongated, the respective stretching frequency is red-shifted, and the intensity of the corresponding spectral band systematically increases. It is important to note that only changes in stretching vibration frequencies and the intensity of the respective spectral bands are observable, as changes in bond length cannot be detected in the gas phase. These features are widely used to identify the existence of H-bonds and represent a fingerprint of H-bond formation[7].

Previously, we investigated hydridic H-bonded complexes formed by Me_3SiH and several electron acceptors both experimentally and computationally[15], and hydridic H-bonded complexes formed by transition metal hydrides and several electron acceptors computationally[16]. However, a direct comparison of protonic and hydridic H-bonds based on both reliable experimental and calculated data is still lacking.

[1]Institute of Organic Chemistry and Biochemistry of the Czech Academy of Sciences, Prague 6, Czech Republic. [2]IT4Innovations, VŠB-Technical University of Ostrava, Ostrava-Poruba, Czech Republic. [3]J. Heyrovský Institute of Physical Chemistry, Czech Academy of Sciences, Prague 8, Czech Republic.
✉e-mail: svatopluk.civis@jh-inst.cas.cz; pavel.hobza@uochb.cas.cz

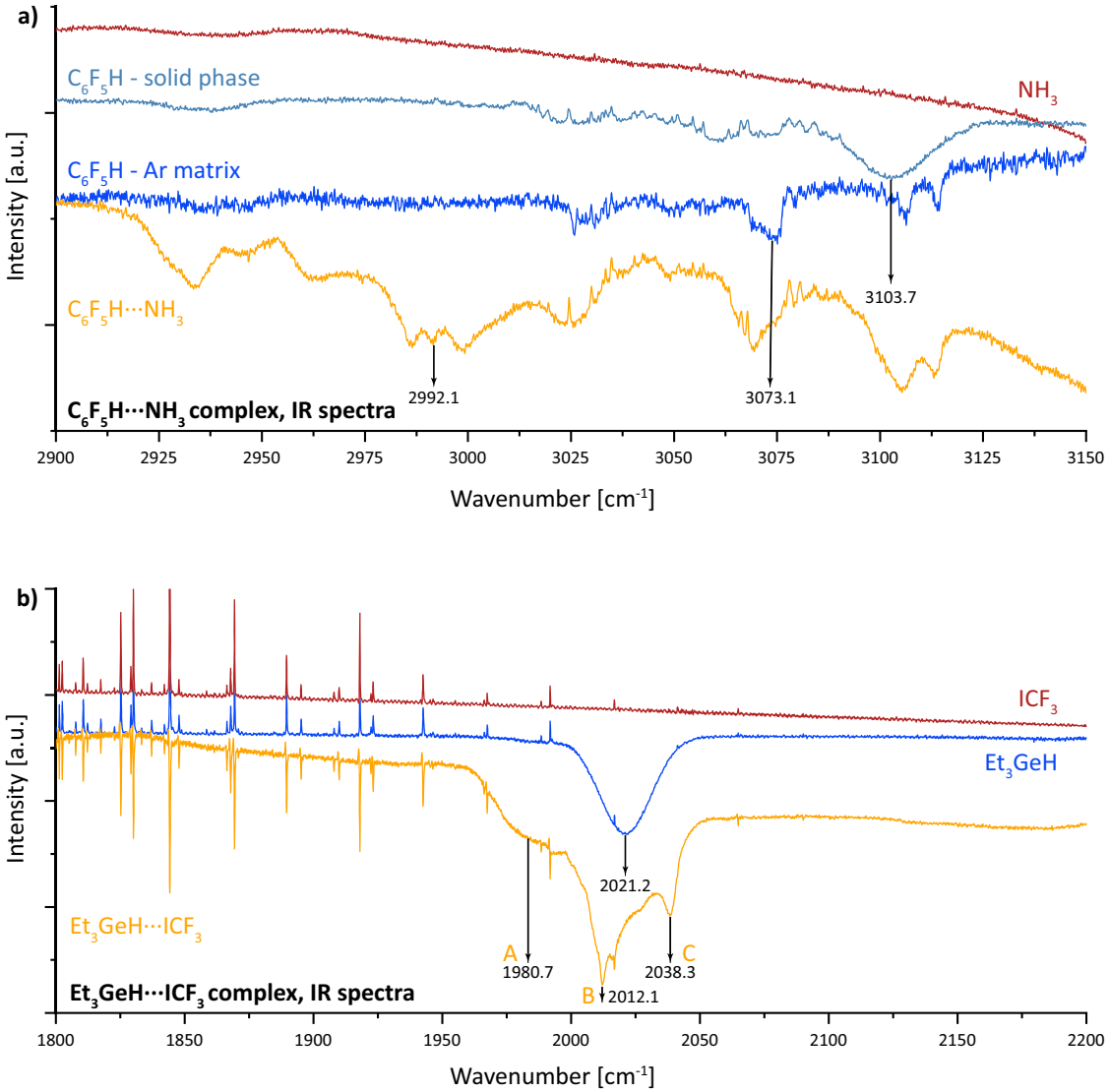

Fig. 1 | Experimental Infrared spectra of investigated complexes, $C_6F_5H\cdots NH_3$ and $Et_3GeH\cdots ICF_3$ measured in the argon matrix. a provides spectrum of $C_6F_5H\cdots NH_3$ complex in yellow, C_6F_5H monomer in blue and NH_3 monomer in red. The C_6F_5H solid phase spectrum is also presented for the sake of comparison in light blue. **b** provides spectrum of $Et_3GeH\cdots ICF_3$ in yellow, Et_3GeH monomer in blue and ICF_3 monomer in red. The narrow lines in the red, blue and yellow spectra depicted in panel (**b**) correspond to the atmospheric water absorption.

The aim of the present paper is to investigate experimentally (using low-temperature IR spectroscopy) and computationally the origin and consequences of changes in electron density in electron donors and acceptors during the formation of protonic and hydridic H-bonds in $C_6F_5H\cdots NH_3$ and $Et_3GeH\cdots ICF_3$ complexes. In the first complex, hydrogen is protonic, while in the second, it is hydridic. Electronic changes accompanying the formation of both complexes are rather small, and to prevent misinterpretation of the data obtained, we used in both cases identical and as accurate as possible experimental and computational tools.

Systems considered

For calculations of hydridic hydrogen bond complexes, we selected Me_3SiH, Me_3GeH, Me_3SnH, and Et_3GeH as electron donors. The electron acceptors chosen included molecules with p-holes (BF_3), σ-holes (BrCN, ICF_3, ICN, PCl_3, $P(CN)_3$, and $S(CN)_2$), and π-holes ($C_6(CN)_3H_3$, COF_2, and NO_2F). To compare these with protonic hydrogen bond complexes, we selected H-bonded complexes from a reference[16] and complexes from another study[17,18] with comparable ΔE to the hydridic hydrogen-bonded ones. Specifically, we chose complexes of ammonia with acetaldehyde and nitrosomethane; ethyne with acetaldehyde and acetone; hydrogen fluoride with acetone; hydrogen chloride with methanol and phosphorine; hydrogen bromide and hydrogen iodide with dimethyl sulfoxide, N-methylacetamide, tetrahydrothiophene, tetrahydroselenophene, tetrahydrotellurophene, trimethyl phosphate, and trimethylphosphine; methanethiol with methanol and phosphorine; methanol with acetamide and methylazide; pentafluorobenzene with acetone, ammonia, nitrosomethane, and trimethylphosphine; and water with furan and nitrosomethane.

Results and discussion

IR experiments

Orange spectrum in Fig. 1a, belongs to a mixture of Ar (500 parts), C_6F_5H (1 part) and NH3 (1 part by volume) obtained by supersonic expansion of this mixture on a KBr window cooled to 20 K. Comparison with this spectrum are C_6F_5H spectra measured in an argon matrix (blue) and spectrum of pure ammonia (red). In addition, the spectrum of C_6F_5H measured after direct injection of this substance onto a cooled window made of KBr material is added to the figure.

The picture shows a broad peak of C_6F_5H at 3103.7 cm^{-1} which belongs to C_6F_5H in the solid phase in the form of ice. The spectrum of the $C_6F_5H\cdots NH_3$ system is relatively complex and breaks down into a number

of relatively broad peaks that partly belong to the complex itself, but also to individual unreacted components. It turned out that in a number of our experiments it is very important to estimate stoichiometrically the ratio (mixture) of the individual components forming the complex. It often happens that during the formation of a molecular complex, some unreacted molecules are excluded from the reaction and appear in the spectrum as individual components. The spectral lines of these unreacted molecules can easily be identified based on previously measured individual spectra. From the argon-matrix spectra we attributed the peak around 3073 cm^{-1} to the C_6F_5H monomer, and the peak around 2992 cm^{-1} to the $C_6F_5H\cdots NH_3$ complex, with the resulting redshift of the C-H stretching frequency being 40.5 cm^{-1}.

Figure 1b shows the spectrum of pure Et_3GeH in an argon matrix (blue), the spectrum of pure ICF_3 in an argon matrix (red), and the spectrum of the Ar–$Et_3GeH\cdots ICF_3$ mixture (1000:1) at 55 K (orange). The single peak around 2021.2 cm^{-1} at the blue curve is attributed to the Ge-H stretching frequency in the isolated Et_3GeH monomer. Three peaks at 1980.7, 2012.1, and 2038.3 cm^{-1} at the orange curve correspond to the Ge-H stretching frequencies in the A, B and C structures (Fig. S1 and the following text) of the $Et_3GeH\cdots ICF_3$ complex. We assigned the resulting redshift of 40.5 cm^{-1} to the hydridic hydrogen bond in the structure A, where the hydridic hydrogen from Et_3GeH interacts with the positive σ-hole on ICF_3. A redshift of 9.1 cm^{-1} was assigned to the structure B where the CF_3 fragment from the ICF_3 molecule interacts with the ethyl groups of Et_3GeH. Lastly, a blueshift of 17.1 cm^{-1} was assigned to the dispersion-driven structure C where iodine from ICF_3 interacts with ethyl groups of Et_3GeH. Complexes B and C are not the main interest of this study and are therefore not discussed further.

It should be noted that all spectra were measured in a cryostat freely inserted into the sample chamber of the Vertex spectrometer under atmospheric air pressure in the laboratory. For these reasons, narrow absorption lines of atmospheric water appear in the spectrum, which were then used in the pre-calibration of the individual spectra.

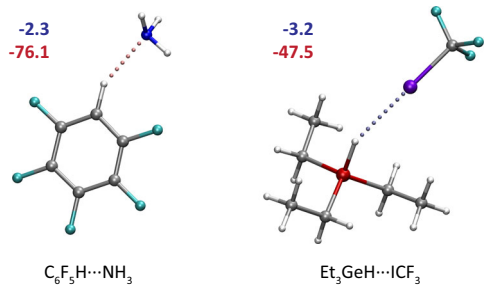

Fig. 2 | Structures of protonic H-bonded $C_6F_5H\cdots NH_3$ and hydridic H-bonded $Et_3GeH\cdots ICF_3$ complexes optimized at MP2/aug-cc-pwCVTZ (aug-cc-pwCVTZ-PP for Ge and I) level of theory. Interaction free energies (in kcal.mol^{-1}) are depicted in blue while the red shifts of X-H stretching frequency (in cm^{-1}) are depicted in red.

Calculations

Subsystems. Table S1 provides a summary of the atomic charges for all hydrogen donors (both protonic and hydridic) discussed in this paper. As expected, the X-H hydrogens in the Me_3XH (X = Si, Ge, Sn) and Et_3GeH subsystems exhibit hydridic character, whereas the hydrogens in other donors are protonic. Additionally, the data in Table S1 shows that the NBO charges, which are primarily used in the subsequent analysis, show a strong correlation with those derived from alternative methods, such as Hirshfeld or RESP.

Complexes. Structures of the $C_6F_5H\cdots NH_3$ and $Et_3GeH\cdots ICF_3$ complexes, which exhibit protonic and hydridic H-bonds respectively, are shown in Fig. 2. The structure, energy, and vibrational characteristics are summarized in Table 1. Table S2 shows energy and vibration characteristic of all three structures of the latter complex (cf Fig. S1). Clearly, structure A corresponds to the global minimum with binding free energy of 3.2 kcal.mol^{-1} and only it will be considered in the forthcoming discussion. Our intention was to compare protonic and hydridic H-bonded complexes with similar stabilization energies, and Table 1 demonstrates that the present selection was successful. Both complexes exhibit comparable stability, as evidenced by their calculated interaction and binding free energies. The binding free energies of both complexes at 50 K are positive (stabilizing), indicating that both complexes will be populated at this experimental temperature. Moreover, the difference in binding free energies, with the first complex having a larger value, is attributed to entropy.

The main finding of this study is related to the shift in the X-H stretching frequency, which serves as a fingerprint for H-bond formation. IR experiments on both complexes reveal significant red shifts, with the shift being slightly larger for the protonic H-bond. The calculated spectral shifts agree fairly well with the experimental values, providing evidence for the accuracy of the theoretical treatment. In addition to the shifts in stretching frequencies, the H-bond is also manifested by an increase in the intensity of the respective spectral band. Since the current experimental setup does not allow for the detection of spectral band intensity, we determined it computationally (see Table 1). The intensity increase is significant in both complexes and comparable.

The comparable changes in stretching frequencies and intensities of spectral bands upon complex formation, regardless of whether the hydrogen is protonic or hydridic, are indeed surprising. This is because systems with protonic and hydridic hydrogens exhibit different directions of charge transfer. In hydridic hydrogen systems, such as triethylgermane, the molecule acts as an electron donor, while in protonic hydrogen systems, like pentafluorobenzene, the molecule acts as an electron acceptor.

The spectral red shifts are primarily attributed to the weakening and elongation of the X-H bond upon complex formation, with the change in bond length being a key quantity. Since experimental determination of geometry changes for these complexes in the gas phase is not feasible, we are limited to computational methods. Table 1 reveals that the X-H bond was elongated in both complexes, by 0.005 and 0.009 Å, respectively. To verify these values obtained at the correlated MP2 level, we employed various

Table 1 | Interaction energy and interaction free energy, changes of the X-H stretching frequency and its intensity, population of the σ bonding and σ* antibonding orbitals and the X-H bond distance upon complex formation, and total charge at XH subsystem for complexes with hydridic and protonic H-bonds optimized at the MP2/aug-cc-pwCVTZ (aug-cc-pwCVTZ-PP for Ge and I)[a]

$Et_3GeH\cdots ICF_3$								
ΔE^T	ΔG(50 K)	$\Delta\nu^{CALC}$	$\Delta\nu^{EXP}$	ΔI^{CALC}	Δσ(X-H)	Δσ*(X-H)	Δr(X-H)	Q(XH)[b]
−5.16	−3.20	−47.5	−40.5	148.8	−0.014	0.006	0.009	0.003
$C_6F_5H\cdots NH_3$								
ΔE^T	ΔG(50 K)	$\Delta\nu^{CALC}$	$\Delta\nu^{EXP}$	ΔI^{CALC}	Δσ(X-H)	Δσ*(X-H)	Δr(X-H)	Q(XH)[c]
−4.42	−2.32	−76.1	−81.0	166.5	−0.007	0.033	0.005	−0.014

[a]Energies in kcal.mol^{-1}, Δν in cm^{-1}, Δ*I* in km.mol^{-1}, Δr in Å, Δσ, Δσ* and Q(XH) in electrons, [b] and [c] is the total charge at Et_3GeH and C_6F_5H, respectively.

Table 2 | Selected characteristics of hydridic H- bonded complexes evaluated at the MP2/aug-cc-pwCTZ (aug-cc-pwCVTZ-PP for Ge, Br, Sn, and I) level[a]

Complex	Type of interaction	Δν	Δr(X-H)	Δσ(X-H)	Δσ*(X-H)
$Me_3SiH\cdots BF_3$	SiH···B	−30.8	0.007	−0.009	0.005
$Me_3SiH\cdots BrCN$	SiH···Br	−46.9	0.008	−0.011	0.004
$Me_3SiH\cdots C_6(CN)_3H_3$	SiH···π-hole	−7.6	0.004	−0.004	0.004
$Me_3SiH\cdots COF_2$	SiH···π-hole	−23.9	0.005	−0.003	0.003
$Me_3SiH\cdots ICF_3$	SiH···I	−47.1	0.005	−0.012	0.004
$Me_3SiH\cdots ICN$	SiH···I	−68.8	0.007	−0.018	0.006
$Me_3SiH\cdots NO_2F$	SiH···π-hole	−20.9	0.011	−0.002	0.003
$Me_3SiH\cdots PCl_3$	SiH···P	−31.0	0.005	−0.010	0.006
$Me_3SiH\cdots P(CN)_3$	SiH···P	−98.2	0.005	−0.030	0.011
$Me_3SiH\cdots S(CN)_2$	SiH···S	−58.3	0.016	−0.014	0.006
$Me_3GeH\cdots BF_3$	GeH···B	−37.5	0.008	−0.009	0.004
$Me_3GeH\cdots BrCN$	GeH···Br	−42.1	0.008	−0.011	0.005
$Me_3GeH\cdots C_6(CN)_3\ H_3$	GeH···π-hole	−5.0	0.003	−0.005	0.005
$Me_3GeH\cdots COF_2$	GeH···π-hole	−27.7	0.006	−0.003	0.003
$Me_3GeH\cdots ICF_3$	GeH···I	−48.9	0.006	−0.013	0.005
$Me_3GeH\cdots ICN$	GeH···I	−70.9	0.009	−0.020	0.007
$Me_3GeH\cdots NO_2F$	GeH···π-hole	−26.2	0.013	−0.002	0.003
$Me_3GeH\cdots PCl_3$	GeH···P	−33.1	0.006	−0.015	0.008
$Me_3GeH\cdots P(CN)_3$	GeH···P	−107.7	0.005	−0.012	0.013
$Me_3GeH\cdots S(CN)_2$	GeH···S	−62.7	0.019	−0.015	0.006
$Me_3SnH\cdots BF_3$	SnH···B	−39.3	0.011	−0.009	0.004
$Me_3SnH\cdots BrCN$	SnH···Br	−52.8	0.012	−0.013	0.004
$Me_3SnH\cdots C_6(CN)_3\ H_3$	SnH···π-hole	−10.1	0.005	−0.005	0.002
$Me_3SnH\cdots COF_2$	SnH···π-hole	−22.4	0.008	−0.003	0.002
$Me_3SnH\cdots ICF_3$	SnH···I	−52.8	0.008	−0.016	0.001
$Me_3SnH\cdots ICN$	SnH···I	−79.9	0.011	−0.025	0.007
$Me_3SnH\cdots NO_2F$	SnH···π-hole	−30.3	0.018	−0.002	0.011
$Me_3SnH\cdots PCl_3$	SnH···P	−36.9	0.008	−0.015	0.001
$Me_3SnH\cdots P(CN)_3$	SnH···P	−121.1	0.008	−0.045	0.008
$Me_3SnH\cdots S(CN)_2$	SnH···S	−66.5	0.027	−0.017	0.017

[a]Δν in cm^{-1}, Δr in Å, Δσ and Δσ* in electrons.

computational techniques, including different DFT functionals (wB97M-V and PBE0). As shown in Table S3, all these techniques provided X-H bond elongations comparable to those listed in Table 1.

Tables S4–S7 present data for 30 protonic and 30 hydridic H-bonded complexes determined at the MP2 level with stabilization energies ranging from 3.0 to 10.9 kcal.mol^{-1} and 3.5 to 8.0 kcal.mol^{-1}, respectively. Structures of all complexes investigated are depicted on the Figs. S2–S6. This range covers weak, medium, and strong H-bonds, and it is noteworthy that all X-H bond lengths were systematically elongated, with comparable elongation observed for both types of H-bonded complexes.

An important question arises: what is the reason for this systematic elongation of the X-H bond? To address this, we performed NBO analysis. Tables 1, 2, 3, and Tables S3–S15 confirm the well-known fact that, in protonic H-bonding, charge transfer from the electron donor is directed to the X-H σ* antibonding orbital, leading to its weakening and elongation. The X-H system thus behaves as a Lewis acid. Table 1 shows for protonic H-bond a significant increase (by 0.033 e) in electron density in the C-H σ* antibonding orbital. In contrast, for hydridic H-bond, Table 1 indicates that the largest change does not concern an increase in the Ge-H σ* antibonding orbital, but a decrease in electron density in the Ge-H σ bonding orbital (−0.014 e). The X' – H system thus now behaves as a Lewis base. This trend is consistent across all 30 hydridic and 30 protonic H-bond complexes listed in Tables S3–S15. The NBO analysis across all these complexes unambiguously confirms that the electron density in the X-H σ* orbitals of protonic complexes systematically increase, while electron density in the X-H σ orbitals of hydridic complexes systematically decreases and we are aware of the fact that the changes in populations of σ bonding and σ* antibonding orbitals are for the complexes with hydridic H-bonds smaller. Correlation between increase in population of σ* antibonding orbitals and the respective red shift of the X-H stretching frequency in complexes with protonic H-bond given in Table 3 is closer than that between decrease in population of σ bonding orbitals and the respective red shift of the X-H stretching frequency in complexes with hydridic H-bond presented in Table 2 (0.9 and 0.7). Explanation of this fact is due to the different role of charge transfer, electrostatic, induction and dispersion energy components. In the case of protonic H-bonds the leading role of electrostatic energy is well recognized. Recently we published the paper[16] where we studied different transition metal containing complexes with hydridic H-bonds. In all complexes investigated the dispersion energy represented the dominant energy components what was explained by the partial negative charge at

Table 3 | Selected characteristics of protonic hydrogen bond complexes evaluated at the MP2/aug-cc-pwCTZ (aug-cc-pwCVTZ-PP for Se, Br, Te, and I) level[a]

Complex	HB type	Δν	Δr(X-H)	Δσ(X-H)	Δσ*(X-H)
NH_3···MeCHO	NH···O	−37.4	0.004	−0.001	0.006
NH_3···MeNO	NH···O	−20.8	0.002	−0.001	0.003
C_2H_2···MeCHO	CH···O	−57.0	0.006	−0.001	0.008
C_2H_2···Me_2CO	CH···O	−71.3	0.007	−0.002	0.010
HF···Me_2CO	FH···O	−569.1	0.026	0.000	0.050
HCl···MeOH	ClH···O	−396.3	0.028	−0.002	0.043
HCl···C_5H_5P	ClH···P	−192.1	0.013	−0.002	0.035
HBr···Me_2SO	BrH···O	−633.1	0.052	−0.006	0.078
HBr···C_3H_7NO	BrH···O	−457.6	0.038	−0.006	0.060
HBr···$(CH_2)_4S$	BrH···S	−721.3	0.060	−0.006	0.135
HBr···$(CH_2)_4Se$	BrH···Se	−629.1	0.051	−0.005	0.127
HBr···$(CH_2)_4Te$	BrH···Te	−556.9	0.045	−0.005	0.121
HBr···$(OMe)_3PO$	BrH···O	−458.7	0.038	−0.005	0.055
HBr···Me_3P	BrH···P	−606.3	0.048	−0.005	0.127
HI···Me_2SO	IH···O	−689.0	0.067	−0.010	0.095
HI···C_3H_7NO	IH···O	−369.4	0.036	−0.008	0.059
HI···$(CH_2)_4S$	IH···S	−871.4	0.095	−0.012	0.193
HI···$(CH_2)_4Se$	IH···Se	−740.5	0.075	−0.009	0.172
HI···$(CH_2)_4Te$	IH···Te	−655.8	0.065	−0.009	0.164
HI···$(OMe)_3PO$	IH···O	−389.2	0.037	−0.008	0.056
HI···Me_3P	IH···P	−701.0	0.068	−0.009	0.165
MeSH···MeOH	SH···O	−19.1	0.002	−0.001	0.004
MeSH···C_5H_5P	SH···P	−19.9	0.002	−0.002	0.005
MeOH···C_2H_5NO	OH···O	−86.8	0.012	0.000	0.023
MeOH···MeN_3	OH···N	−114.3	0.006	−0.002	0.011
C_6F_5H···Me_2CO	CH···O	−55.1	0.004	−0.007	0.008
C_6F_5H···MeNO	CH···O	−8.3	0.001	−0.005	0.002
C_6F_5H···Me_3P	CH···P	−69.2	0.005	−0.006	0.015
H_2O···C_4H_4O	OH···O	−23.7	0.004	−0.001	0.005
H_2O···MeNO	OH···O	−30.9	0.005	0.000	0.011

[a]Δν in cm^{-1}, Δr in Å, Δσ and Δσ* in electrons.

hydridic hydrogens. The SAPT calculations performed for the present set of complexes with hydridic and protonic H-bonds (Tables 2 and 3) fully confirmed this findings. Specifically, Tables S16, S17 and S18 present SAPT(2 + 3) energy decomposition for complexes with hydridic H-bonds and in all cases the dispersion energy is more attractive than the electrostatic one. Table S19 shows the energy decomposition for complexes with protonic H-bond and in all but two complexes the electrostatic energy is clearly dominant.

Tables S3–S15 further demonstrate that the X-H stretching frequency for all electron donors is systematically red-shifted upon complex formation, with a corresponding increase in the intensity of the spectral band. From Tables S3–S15, it is further evident that these findings hold consistently without exception. This conclusion is crucial as it shows that the dominant changes in electron density in systems with protonic and hydridic H-bonds, upon complex formation, act in the same direction. Specifically, an increase in electron density in the antibonding orbital of protonic H-bonded complexes and a decrease in electron density in the bonding orbital of hydridic H-bonded complexes both lead to the weakening and elongation of the X-H bond and a red shift in the respective stretching frequency.

The experimental and computational analyses of C_6F_5H···NH_3 and Et_3GeH···ICF_3 complexes, which feature protonic and hydridic H-bonds revealed a surprising result: despite the opposite directions and different origin of charge transfer in protonic and hydridic hydrogen bonds, their spectral characteristics -specifically, the red shift of the X-H stretching frequency and the increase in intensity upon complex formation- are remarkably similar. Additional computational analyses performed on 30 protonic and 30 hydridic H-bonded complexes fully confirmed the above mentioned results. This observation is a key characteristic that unifies protonic and hydridic H-bonding, supporting the formulation of a new, unified definition of H-bonding.

Nomenclature. The IUPAC definition of hydrogen bonding recognizes only one type of H-bond, which we referred to earlier as the protonic H-bond. The definition does not encompass the other type, known as the hydridic H-bond, because it specifies that hydrogen in an H-bond must be covalently bound to an electronegative atom and thus bears a partial positive charge, and, further, the dominant energy term must be electrostatic. Consequently, alternative names such as "hydride bond"[13], "charge-inverted H-bond"[8–11,19], "inverse H-bond"[12], or our term "hydridic H-bond"[15,16] are fundamentally at odds with the existing IUPAC definition.

For some, but not all, types of hydridic H-bonds studied here and elsewhere, the term "halogen bond" may be appropriate. However, it is important to note that there are complexes where hydridic hydrogen interacts with p-holes, π-holes, and various σ-holes, not exclusively those on halogens. For instance, the Et_3GeH···ICF_3 complex investigated in this study could be alternatively referred to as an H···I σ-hole halogen bonded complex. The formation of this halogen bond is accompanied by a small to negligible red shift in the I-C stretching frequency (3 cm^{-1}) and a negligible change in the intensity of the corresponding spectral band. These changes are subtle and may be difficult or impractical to detect. Conversely, when considering the complex as an H-bonded system, the red shift of the Ge-H stretching frequency (−47.5 cm^{-1}) and the significant increase in intensity (148.8 km/mol) are substantial, making their IR detection routine and straightforward. We ask the question whether it is better to use for this and similar complexes the name of halogen bond where experimental detection of the respective properties would be difficult or even impractical.

There are three potential solutions to handle the nomenclature issue:

(i) to keep the current definition of H-bond as it is with no other action. Based on several discussions invoked by our lectures on this topic we find out this being preferred.

(ii) To keep the current IUPAC definition and introduce a completely new term for bonds involving hydridic hydrogen. Since the term "H-bond" is already reserved for the original definition, this would require the introduction of a new term (e.g., hydride bond as suggested by Grabowski et al.[13]) which does not contain "H-bond' in any version.

(iii) To modify the existing 2011 IUPAC definition of hydrogen bonding to cover both protonic and hydridic H-bonds. Although it is generally not easy to make any change in definition and it requires extensive scientific discourse, the necessary modifications which we suggest are relatively easy to implement. In this connection, one of us (PH) recalls a very friendly and productive atmosphere in Pisa in 2005, where the current IUPAC definition of the H-bonding was established. This definition was triggered by the discovery that the H-bonding can be evidenced not only by a red shift of the X-H stretching frequency but also by a blue shift.

We are certainly aware that before changing the definition of hydrogen bonding considerably more data, both experimental and computational, should be collected and carefully analyzed with the aim to be more unambiguously convincing. In our first paper on hydridic H-bonding published in J. Am. Chem. Soc.[15] we noted that " any change of existing definition is difficult and cannot be rushed and required an extended, broad, and in-depth discussion within the scientific community".

Methods

IR experiment

In our low-temperature IR experiments, we employed two different approaches (for more details, see the SI). The first approach involves the technique of direct spectral measurement of a supersonically expanded mixture of reaction intermediates on a cold substrate, referred to as the solid-phase complex (SPC) method. The second approach utilizes the technique of noble-gas matrix isolation (MI).

The procedure of low-temperature experiments was described elsewhere[20]. The gas mixtures are deposited onto a cooled KBr substrate of the cryostat at a temperatures between 18–70 K. The relative concentrations of the products were monitored using integrated absorption intensities of the selected infrared bands. The intermediates which are parts of low temperature complex have been supersonically expand into the high vacuum (10^{-6} Torr) on cold 18 K substrate (minimal attainable temperature) inside of Leybold cryostat chamber. The spectra were obtained by use of the Bruker Vertex spectrometer with KBr optics, HgCdTe detector and a KBr beam splitter. The broad spectral region was cut by optical interference filters with transparency in the range of 700–5000 cm^{-1}. The KBr entry window of the spectrometer was used. The unapodized spectral resolution was 0.06 cm^{-1}. Between 30 and 100 scans, depending on the sample, were coadded so as to obtain a reasonable signal-to-noise ratio. The observed wavenumbers were calibrated using H_2O absorption rotation-vibration lines presented in the spectrum.

Matrix isolation is a well-known technique frequently used for the measurement of unstable species such as ions, radicals, and low-temperature molecular complexes in a cold matrix of noble gas (Ng). Similar to the first approach, a mixture of reaction intermediates combined with argon gas (molar ratio 1:1000) is expanded through a pulse nozzle onto the cold (20 K) KBr substrate, and the spectra are recorded using the Bruker Vertex spectrometer.

Computations

Geometries of all subsystems and complexes were optimized at the RI-MP2/aug-cc-pwCVTZ[21] level (aug-cc-pwCVTZ-PP[22] for Ge, Se, Br, Sn, Te, and I), the ωB97M-V[23]/aug-cc-pwCVTZ level (aug-cc-pwCVTZ-PP for Ge, Se, Br, Sn, Te, and I), and the PBE0[24]/def2-TZVPPD[25] level with an additional D4[26] dispersion correction. Harmonic vibration frequencies, evaluated under the rigid rotor-harmonic oscillator-ideal gas approximation, were determined at the same theoretical levels. Natural Bond Orbital (NBO) analyses were performed with the NBO7[27,28] program at the same levels as the geometry optimizations. These calculations were carried out using the ORCA 5.0.4[29] software and Molpro 2024.1[30,31]. Hirshfeld population[32] analysis was conducted using ORCA 5.0.4 with the PBE0/def2-TZVPPD method. Restricted electrostatic potential (RESP) charges[33] were calculated at the PBE0/def2-TZPPD level of theory, utilizing the Q-Chem 6.2[34] software package. Symmetry-adapted perturbation theory[35] (SAPT) were performed using the aug-cc-pwCVTZ basis set for all atoms with atomic numbers less than 32. For Ge, Se, and Br atoms, the all-electron aug-cc-pVTZ[36] basis set was employed due to convergence issues encountered with the aug-ccpwCVTZ-PP basis set. For Sn, Te, and I atoms, the aug-cc-pwCVTZ-PP basis set was applied. All SAPT calculations were executed using the PSI4 1.9.1[37] software package.

Supplementary information

Figure S1 provides three structures of the $Et_3GeH\cdots ICF_3$ possessing hydridic H-bond, Figures S2–S6 provides pictures of all studied complexes. Tables S1–S15 collect charge, energy and vibration characteristics of selected complexes with protonic and hydridic H-bonds. Tables S16–S19 collects SAPT 2 + 3 results for all studied complexes.

Data availability

Authors can confirm that all relevant data are included in the paper and its supplementary information files.

Received: 7 August 2024; Accepted: 18 October 2024;
Published online: 07 November 2024

References

1. Černý, J. & Hobza, P. Non-covalent interactions in biomacromolecules. *Phys. Chem. Chem. Phys.* **9**, 5291–5303 (2007).
2. Grabowski, S. J. What is the covalency of hydrogen bonding? *Chem. Rev.* **111**, 2597–2625 (2011).
3. Gerlt, J. A., Kreevoy, M. M., Cleland, W. W. & Frey, P. A. Understanding enzymic catalysis: the importance of short, strong hydrogen bonds. *Chem. Biol.* **4**, 259–267 (1997).
4. Řezáč, J. & Hobza, P. Benchmark calculations of interaction energies in noncovalent complexes and their applications. *Chem. Rev.* **116**, 5038–5071 (2016).
5. Hobza, P. et al. Anti-hydrogen bond between chloroform and fluorobenzene. *Chem. Phys. Lett.* **299**, 180–186 (1999).
6. Hobza, P. & Havlas, Z. Blue-shifting hydrogen bonds. *Chem. Rev.* **100**, 4253–4264 (2000).
7. Arunan, E. et al. Defining the hydrogen bond: an account (IUPAC Technical Report). *Pure Appl. Chem.* **83**, 1619–1636 (2011).
8. Jabłoński, M. Binding of X-H to the lone-pair vacancy: charge-inverted hydrogen bond. *Chem. Phys. Lett.* **477**, 374–376 (2009).
9. Jabłoński, M. Theoretical insight into the nature of the intermolecular charge-inverted hydrogen bond. *Comput Theor. Chem.* **998**, 39–45 (2012).
10. Jabłoński, M. Comparative study of geometric and QTAIM-based differences between X–H···Y intramolecular charge-inverted hydrogen bonds, M1···(H–X) agostic bonds and M2···(η2-XH) σ interactions (X = Si, Ge. *Comput. Theor. Chem*. **1096**, 54–65 (2016).
11. Jabłoński, M. Ten years of charge-inverted hydrogen bonds. *Struct. Chem.* **31**, 61–80 (2020).
12. Rozas, I., Alkorta, I. & Elguero, J. Inverse hydrogen-bonded complexes. *J. Phys. Chem. A* **101**, 4236–4244 (1997).
13. Grabowski, S. J., Sokalski, W. A. & Leszczynski, J. Hydride bonding—Ab initio studies of BeH2…Li+, BeH2…Na+ and BeH2…Mg2+ model systems. *Chem. Phys. Lett.* **422**, 334–339 (2006).
14. Grabowski, S. J. Hydrogen bond types which do not fit accepted definitions. *Chem. Commun.* **60**, 6239–6255 (2024).
15. Civiš, S. et al. Hydrogen bonding with hydridic hydrogen-experimental low-temperature IR and computational study: is a revised definition of hydrogen bonding appropriate? *J. Am. Chem. Soc.* **145**, 8559 (2023).
16. Lamanec, M., Zienertová, J., Špeťko, M., Nachtigallová, D. & Hobza, P. Similarities and differences of hydridic and protonic hydrogen bonding. *ChemPhysChem* **25**, e202400403 (2024).
17. Řezáč, J. Non-covalent interactions atlas benchmark data sets: hydrogen bonding. *J. Chem. Theory Comput* **16**, 2355–2368 (2020).
18. Řezáč, J. Non-covalent interactions atlas benchmark data sets 2: hydrogen bonding in an extended chemical space. *J. Chem. Theory Comput.* **16**, 6305–6316 (2020).
19. Jabłoński, M. Charge-inverted hydrogen bond vs. other interactions possessing a hydridic hydrogen atom. *Chem. Phys.* **433**, 76–84 (2014).
20. Bondybey, V. E., Smith, A. M. & Agreiter, J. New developments in matrix isolation spectroscopy. *Chem. Rev.* **96**, 2113–2134 (1996).
21. Peterson, K. A. & Dunning, T. H. Accurate correlation consistent basis sets for molecular core–valence correlation effects: The second row atoms Al–Ar, and the first row atoms B–Ne revisited. *J. Chem. Phys.* **117**, 10548 (2002).
22. Peterson, K. A. & Yousaf, K. E. Molecular core-valence correlation effects involving the post-d elements Ga-Rn: Benchmarks and new pseudopotential-based correlation consistent basis sets. *J. Chem. Phys.* **133**, 174116 (2010).

23. Mardirossian, N. & Head-Gordon, M. ω B97M-V: a combinatorially optimized, range-separated hybrid, meta-GGA density functional with VV10 nonlocal correlation. *J. Chem. Phys.* **144**, 214110 (2016).
24. Adamo, C. & Barone, V. Toward reliable density functional methods without adjustable parameters: the PBE0 model. *J. Chem. Phys.* **110**, 6158–6170 (1999).
25. Weigend, F. & Ahlrichs, R. Balanced basis sets of split valence, triple zeta valence and quadruple zeta valence quality for H to Rn: design and assessment of accuracy. *Phys. Chem. Chem. Phys.* **7**, 3297–3305 (2005).
26. Caldeweyher, E., Bannwarth, C. & Grimme, S. Extension of the D3 dispersion coefficient model. *J. Chem. Phys.* **147**, 034112 (2017).
27. Glendening, E. D., Landis, C. R. & Weinhold, F. NBO 7.0: new vistas in localized and delocalized chemical bonding theory. *J. Comput Chem.* **40**, 2234–2241 (2019).
28. Reed, A. E., Weinhold, F., Curtiss, L. A. & Pochatko, D. J. Natural bond orbital analysis of molecular interactions: theoretical studies of binary complexes of HF, H2O, NH3, N2, O2, F2, CO, and CO2 with HF, H2O, and NH3. *J. Chem. Phys.* **84**, 5687 (1998).
29. Neese, F., Wennmohs, F., Becker, U. & Riplinger, C. The ORCA quantum chemistry program package. *J. Chem. Phys.* **152**, 224108 (2020).
30. Werner, H. J., Knowles, P. J., Knizia, G., Manby, F. R. & Schütz, M. Molpro: a general-purpose quantum chemistry program package. *Wiley Interdiscip. Rev. Comput. Mol. Sci.* **2**, 242–253 (2012).
31. Werner, H. J. et al. The Molpro quantum chemistry package. *J. Chem. Phys.* **152**, 144107 (2020).
32. Hirshfeld, F. L. Bonded-atom fragments for describing molecular charge densities. *Theor. Chim. Acta* **44**, 129–138 (1977).
33. Cornell, W. D. & Cieplak, P. Christopher, I, Bayly, I. & Kollman, P. A. Application of RESP charges to calculate conformational energies, hydrogen bond energies, and free energies of solvation. *J. Am. Chem. Soc.* **115**, 9620–9631 (1993).
34. Epifanovsky, E. et al. Software for the frontiers of quantum chemistry: an overview of developments in the Q-Chem 5 package. *J. Chem. Phys.* **155**, 84801 (2021).
35. Jeziorski, B., Moszynski, R. & Szalewicz, K. Perturbation theory approach to intermolecular potential energy surfaces of van der Waals complexes. *Chem. Rev.* **94**, 1887–1930 (1994).
36. Wilson, A. K., Woon, D. E., Peterson, K. A. & Dunning, T. H. Gaussian basis sets for use in correlated molecular calculations. IX. The atoms gallium through krypton. *J. Chem. Phys.* **110**, 7667–7676 (1999).
37. Smith, D. G. A. et al. P SI4 1.4: Open-source software for high-throughput quantum chemistry. *J. Chem. Phys.* **152**, 184108 (2020).

Acknowledgements

This article has been produced with the financial support of the European Union under the REFRESH – Research Excellence for Region Sustainability and High-tech Industries project number CZ.10.03.01/00/22_003/0000048 via the Operational Program Just Transition (M.L. and P.H.), and by the Ministry of Education, Youth and Sports of the Czech Republic through the e-INFRA CZ (ID:90254).

Author contributions

M.L. performed the calculations. S.C. designed and conducted experiments. P.H. supervised the project and wrote the manuscript.

Competing interests

The authors declare no competing interests.

Additional information

Supplementary information The online version contains supplementary material available at https://doi.org/10.1038/s42004-024-01334-9.

Correspondence and requests for materials should be addressed to Svatopluk Civiš or Pavel Hobza.

Peer review information *Communications Chemistry* thanks Shamik Chakraborty, Daniel Sethio, and Ekaterina Pas for their contribution to the peer review of this work. Peer review reports are available.